Check for updates

Removal of amoxicillin from aqueous solution using sludge-based activated carbon modified by walnut shell and nano-titanium dioxide

Xiaorong Kang, Yali Liu, Can Yang and Han Cheng

ABSTRACT

Dewatered municipal sludge was used as raw material to prepare activated carbon (SAC), and the SAC was modified by walnut shell and nano-titanium dioxide (MSAC). The results showed that the MSAC had a higher specific surface area (S_{BET}) (279.147 m^2/g) and total pore volume (V_T) (0.324 cm^3/g) than the SAC. Simultaneously, the functional groups such as C-O, C = O, and Ti-O-Ti on the surface of MSAC were enhanced due to modification. These physicochemical properties provided prerequisites for the diffusion and degradation of pollutants in MSAC. Furthermore, the MSAC was applied to adsorb amoxicillin (AMX) from aqueous solution, in batch experiments, the maximum removal rate (88.19%) was observed at an initial AMX concentration of 30 mg/L, MSAC dosage of 5.0 g/L, pH of 8, contact time of 180 min, and temperature of 25 °C. In addition, the adsorption process was well described by the Freundlich isotherm model and pseudo-second-order kinetic model, indicating that the adsorption of AMX onto MSAC was dominated by multilayer chemisorption. Also, the adsorption thermodynamics suggested that the adsorption process of AMX onto MSAC was endothermic, feasible and spontaneous.

Key words | activated carbon, adsorption kinetics, amoxicillin, dewatered sludge, modification

HIGHLIGHTS

- Sludge-based activated carbon was modified by walnut shell and nano-TiO_2.
- Above 88% of amoxicillin was removed.
- Optimum operational parameters were determined.
- Adsorption process was dominated by multi-layer chemisorption.

Xiaorong Kang (corresponding author)
School of Environmental Engineering,
Nanjing Institute of Technology,
Nanjing 211167,
China
E-mail: *feixiang2004@163.com*

Yali Liu
Han Cheng
School of Civil Engineering,
Nanjing Forestry University,
Nanjing 210037,
China

Can Yang
School of Civil Engineering,
Southeast University,
Nanjing, 211189,
China

This is an Open Access article distributed under the terms of the Creative Commons Attribution Licence (CC BY-NC-ND 4.0), which permits copying and redistribution for non-commercial purposes with no derivatives, provided the original work is properly cited (http://creativecommons.org/licenses/by-nc-nd/4.0/).

doi: 10.2166/wrd.2020.162

Downloaded from http://iwaponline.com/jwrd/article-pdf/11/1/97/842448/jwrd0110097.pdf
by guest

GRAPHICAL ABSTRACT

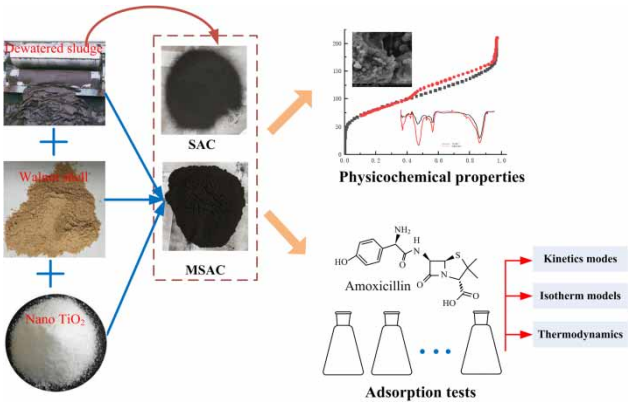

INTRODUCTION

Sludge is an unavoidable by-product of biological treatment in wastewater treatment plants (WWTPs). In 2016, approximately 13 million tons of dry sludge was produced in China (Liu *et al.* 2017b). As sludge contains a large amount of heavy metals, organic pollutants and pathogenic microorganisms, traditional methods for sludge treatment such as landfill, incineration and land application pose huge threats to the environment, economy and human health (Chitongo *et al.* 2019; Wang *et al.* 2019). In recent years, based on the advantages of cheapness, availability, and high organic contents, sludge used as raw material to prepare activated carbon (AC) has been regarded as a sustainable approach of sludge management (Devi & Saroha 2017). Simultaneously, the sludge-based AC (SAC) has been attempted to remove various pollutants such as heavy metals, dyes, and pharmaceuticals from aqueous solution or wastewater (Jin *et al.* 2016; Jaria *et al.* 2019a; Sullivan *et al.* 2019).

Antibiotics have been listed as an important part of emerging organic pollutants, and their pollution to the aquatic environment has become a great concern (Gonzalez-Pleiter *et al.* 2013). As previously reported, continuous discharge of antibiotics into the aquatic environment may have toxic effects on non-target individuals (Gonzalez-Pleiter *et al.* 2013), and their persistence and bioaccumulation also induce long-term risks to aquatic organisms and human health (Kumari & Kumar 2020). For these reasons, tremendous efforts have been made to remove antibiotics from water or wastewater (Silva *et al.* 2018; Li *et al.* 2019c). Among various treatment methods, adsorption is still considered to be the best way to treat antibiotic wastewater, and SAC has shown great potential in removing selected antibiotics (Yang *et al.* 2016; Jaria *et al.* 2019b; Silva *et al.* 2019). Compared with commercial AC, the AC produced from paper mill sludge (PS-AC) exhibited faster adsorption kinetics (15–30 min) for sulfamethoxazole (SMX) (Calisto *et al.* 2015). Chowdhury *et al.* (2019) also demonstrated that the PS-AC effectively adsorbed enrofloxacin (ENF) from solution (95.85%) at an initial concentration of 12 mg/g, an adsorbent dosage of 1.2 g/L, and a contact time of 18 h. In addition, Yao *et al.* (2013) comparatively studied the adsorption effect of sludge source on gatifloxacin (GAT), and the results showed that all SACs had high adsorption capacity for GAT except that made from dried sludge. However, there is scarcity of research concerning the removal of amoxicillin (AMX) using AC prepared from municipal sludge. This may be because high contents of ash and inorganics in the municipal sludge mask the active adsorption sites, resulting in a weak adsorption capacity for organic contaminants (Li *et al.* 2016).

Therefore, the physical and chemical characteristics of SAC should be modified to improve its adsorption capacity (Devi & Saroha 2017). Various agricultural and forestry residues are reported to be much better carbon-rich biomass materials than municipal sludge, containing more lignin and celluloses, and lower ash (Li *et al.* 2016). They are usually,

Downloaded from http://iwaponline.com/jwrd/article-pdf/11/1/97/842448/jwrd0110097.pdf
by guest

therefore, added into sludge to prepare AC samples with large specific surface areas, well-developed pore structures, and strong aromatic groups, which have excellent adsorption capacities for organic pollutants in aqueous solution (Yu *et al.* 2019). On the other hand, the combined use of biochar with nanometallic oxides had high removal capacities for pharmaceuticals (Li *et al.* 2019b; Hassan *et al.* 2020). Some literatures showed that the biochar modified with titanium dioxide (TiO_2) exhibited much higher specific surface area, which increased the interaction between photocatalytic active sites and absorbates (Fazal *et al.* 2019; Li *et al.* 2019a; Silvestri *et al.* 2019). Recently, Li *et al.* (2019a) found that the ultrafine nano-TiO_2 was incorporated into chicken feathers to synthesize light-recycling biochar, and its removal rate for AMX reached 99.97%.

Based on the above research, the main purpose of this study is to evaluate the feasibility of combined modification of walnut shell and nano-TiO_2 for SAC, and the modified SAC (named MSAC) was used to remove AMX from aqueous solution. The MSAC was physically and chemically characterized by scanning electron microscopy (SEM) and Fourier Transform Infrared Spectrometer (FTIR), respectively. Then, the MSAC was tested in batch experiments for the adsorption of AMX, and the effects of five operational parameters, including initial AMX concentration, MSAC dosage, pH, temperature, and contact time, on removal rates were studied. In addition, kinetic models and adsorption isotherm models were investigated to analyze the adsorption mechanism of AMX onto MSAC.

MATERIALS AND METHODS

Raw materials

The dewatered municipal sludge (DMS) used in this test was taken from Qiaobei WWTP in Nanjing, China. Its water content was 79.43%, and the dry weight of volatile solids (VS), ash, C, H, and N were 61.48, 38.52, 25.90, 6.43 and 4.11%, respectively. The walnut shell was purchased from a food company in Nanjing, China. Its characteristics were as follows: VS 98.16%, ash 1.84%, water content 3.57%, C 48.27%, H 6.51% and N 0.34%. These raw materials were dried to constant weight at 105 °C with a drying oven (DGG-9030A, Donglu, Shanghai, China), respectively, and then crushed and sieved through a 40-mesh sieve.

Chemicals

In this study, chemical activating agent $ZnCl_2$ was analytically pure, and the purities of HCl and NaOH were 37 and 96%, respectively. They were provided by Nanjing Chemical Reagent Co. Ltd, Nanjing, China. High-purity nano-TiO_2 and AMX were purchased from Shanghai Mack-Lin Biochemical Technology Co. Ltd, Shanghai, China.

AMX stock solution preparation

A stock solution with concentration of 200 mg/L was prepared by dissolving 0.2 g AMX into 1,000 mL ultra-pure water. Other AMX concentrations required in the experiment were obtained by diluting the stock solution with ultra-pure water.

Preparation of AC samples

In the first step, according to the experimental data (Supplementary material, Figure 1S), the walnut shell, DMS, and nano-TiO_2 were thoroughly mixed in a stainless-steel reactor with a mass ratio of 16:24:1, and then activated with 5.0 M of $ZnCl_2$ solution, the final solid–liquid ratio was 1:3. Second, the mixture was shaken in a thermostatic shaker incubator (SHZ-82, Guohua, Changzhou, China) for 24 h at 25 °C. After shaking, the mixture was centrifuged at 2,352 × g for 5 min, and the sediment was dried in a drying oven at 105 °C to constant weight. Third, the dried mixed solid was pyrolyzed in N_2 atmosphere at 550 °C for 30 min in a resistance furnace (SX-12-10, Xinyi, Shanghai, China), and then cooled to room temperature overnight. Next, the product was washed with 1.0 M HCl, and rinsed with ultra-pure water to neutral pH value. Finally, the prepared MSAC was crushed, ground and sieved to obtain a particle size less than 40 mesh.

The preparation process of SAC was similar to that of MSAC, except that walnut shell and nano-TiO_2 were not added.

Adsorption tests

A series of adsorption studies were conducted in batch mode. The effects of initial AMX concentration (10–90 mg/L), MSAC

Downloaded from http://iwaponline.com/jwrd/article-pdf/11/1/97/842448/jwrd0110097.pdf
by guest

or SAC dosage (1–8 g/L), pH (4–10), contact time (15–180 min), and temperature (15–40 °C) on the adsorption capacity of AMX were studied. In each experiment, only one parameter was changed, and other parameters remained constant. After stirring for a predetermined time interval, 4 mL sample was taken and filtrated through 0.45 μm cellulose acetate membrane (Newstar, Hangzhou Special Paper Industry Co. Ltd, Hangzhou, China), and then the residual AMX concentration in the filtrate was analyzed. The pH values were adjusted by 1.0 M NaOH or HCl solution.

For kinetic studies, 5 g/L of MSAC and SAC were placed in 250 mL Erlenmeyer flasks and contacted with 100 mL of AMX solution (30 mg/L), respectively. The solutions were shaken for different time intervals within 0–180 min. The removal rate (E, %) and the adsorption capacity (q_t, mg/g) of AMX at time t, were calculated by Equations (1) and (2):

$$E = (C_0 - C_t)/C_0 \times 100\% \quad (1)$$

$$q_t = (C_0 - C_t)V/W \quad (2)$$

where C_0 (mg/L) is the initial concentration of AMX (mg/L), and C_t (mg/L) represents the AMX concentration at time t. V(L) is the volume of AMX solution, and W(g) is the weight of MSAC or SAC.

Adsorption isotherm was performed at an MSAC or SAC dosage of 5 g/L and 25 °C by varying initial AMX concentrations (10–90 mg/L). The adsorbed amount of AMX onto MSAC or SAC at the equilibrium, q_e (mg/g), was calculated by Equation (3):

$$q_e = (C_0 - C_e)V/W \quad (3)$$

where C_e (mg/L) is the equilibrium concentration of AMX.

All tests were repeated three times, and the average and standard deviation values were recorded.

Analysis methods

The VS, ash and water content were measured according to Standard Methods (APHA 2001). The analysis of AMX concentration referred to previous literature (Baere & Backer 2007). The pH values were measured using a pH meter (PHS-3C, Leici, Shanghai, China). The elemental compositions of DMS and walnut shell (C, H and N) were analyzed by an automatic elemental analyzer (Vario EL cube, Elementar, Hanau, Germany).

The porosity and surface area characterization of MSAC and SAC were measured by a surface area analyzer (Micrometrics, ASAP2020, Norcross, GA, USA). The surface morphology was observed with a SEM (QUANTA 200, FEI, Hillsboro, OR, USA). The surface functional groups on MSAC and SAC were evaluated by a FTIR spectrometer (IR-360, Nicolet, Madison, WI, USA) with a wavelength range of 400–4,200 cm^{-1}.

RESULTS AND DISCUSSION

Characteristics of AC samples

Physical characterization

The N_2 adsorption/desorption isotherms of SAC and MSAC are shown in Figure 1. It is evident that the isotherm shapes of SAC and MSAC were classified as Type II according to the International Union of Pure and Applied Chemistry (IUPAC) classification (Zhang *et al.* 2016). At $p/p_0 < 0.01$, the N_2 adsorption capacity (63.4 cm^3/g) of MSAC was much higher than SAC (8.9 cm^3/g), indicating that MSAC possessed more micropores (Pal *et al.* 2017). Then, an increase in N_2 adsorption volume was observed with the increase of p/p_0, showing the multilayer adsorption occurred on the outer surfaces of SAC and MSAC (Wang *et al.* 2016). Meanwhile, the hysteresis loops appearing at $p/p_0 > 0.4$ should be attributed to the capillary condensation phenomenon of mesopore structure in SAC and MSAC (Liu *et al.* 2017a).

The pore structure parameters of SAC and MSAC were also analyzed in this study. The specific surface area (S_{BET}) and total pore volume (V_T) of MSAC were 279.147 m^2/g and 0.324 cm^3/g, respectively, which were significantly superior to SAC (35.921 m^2/g and 0.097 cm^3/g). In addition, the average pore size (D_p) of MSAC (4.495 nm) was smaller than SAC (10.425 nm), and the corresponding micropore volume (V_{mic}) of MSAC (0.045 cm^3/g) was more than 11 times that of SAC.

The surface morphology of SAC and MSAC was analyzed by SEM (Figure 2). In comparison to SAC, the

Downloaded from http://iwaponline.com/jwrd/article-pdf/11/1/97/842448/jwrd0110097.pdf
by guest

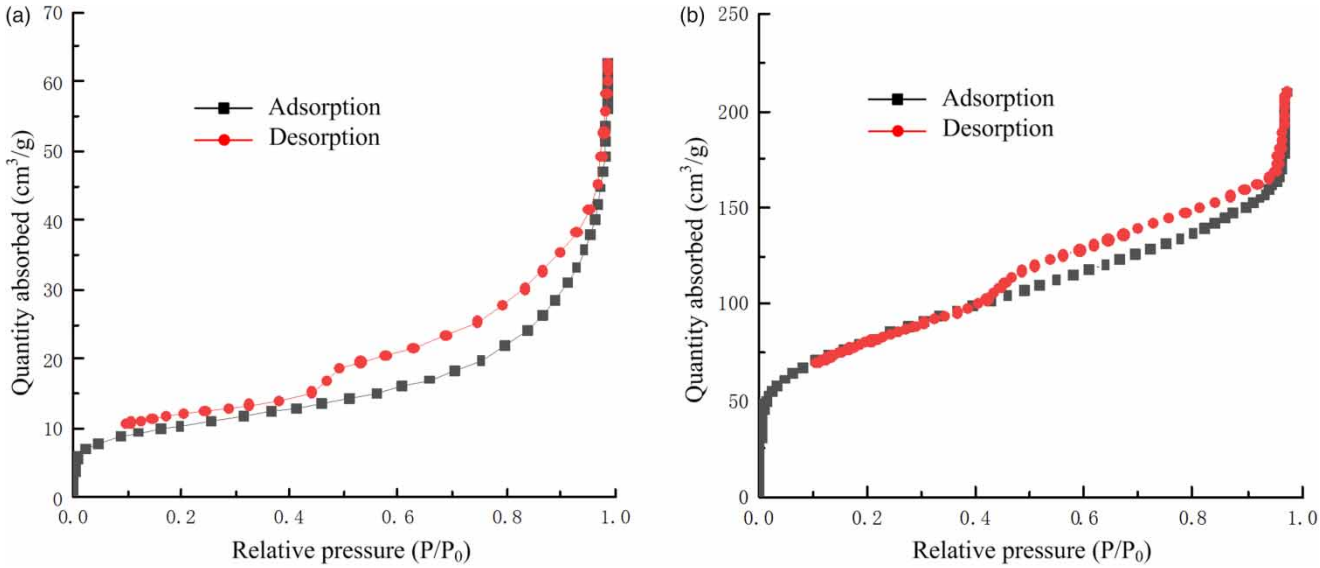

Figure 1 | N_2 adsorption-desorption isotherms of SAC and MSAC.

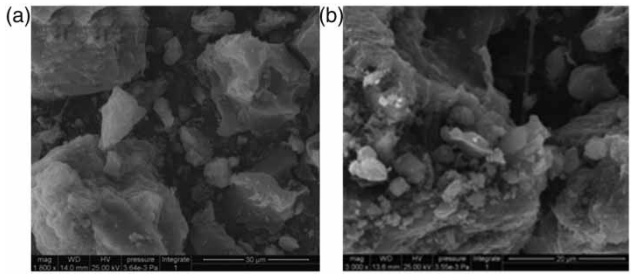

Figure 2 | SEM images of SAC and MSAC.

surface of MSAC exhibited more irregular and looser texture, which also illustrated its large S_{BET} and high porosity. To some extent, the differences between SAC and MSAC explained the effect of combined modification on the formation of porous structures.

In summary, these physical parameters of MSAC revealed that the mesoporous structure provided more channels for AMX to enter the micropores. Simultaneously, the AMX molecules could penetrate into the interior of micropores, because the AMX molecule size is only about 13 Å, which is smaller than the D_p of MSAC.

Chemical characterization

It is reported that the adsorption properties of AC are strongly influenced by its surface functional groups (Salame & Bandosz 2003; Zhang *et al.* 2016). The spectra for SAC and MSAC are depicted in Figure 3. The very broad peak observed at 3,550–3,200 cm^{-1} evidenced the O-H stretching vibrations for carboxyl and phenol (Anisuzzaman *et al.* 2016). A band at 1,685 cm^{-1} could be identified to be C = O, which is associated with carboxylic, lactone and other basic oxygen functional groups such as chromones and pyrone (Gokce & Aktas 2014). The peaks around 1,025 and 1,383 cm^{-1} were derived from the C-O bonds in alcohol and lactone groups, respectively (Gokce & Aktas 2014). More oxygen-containing functional groups

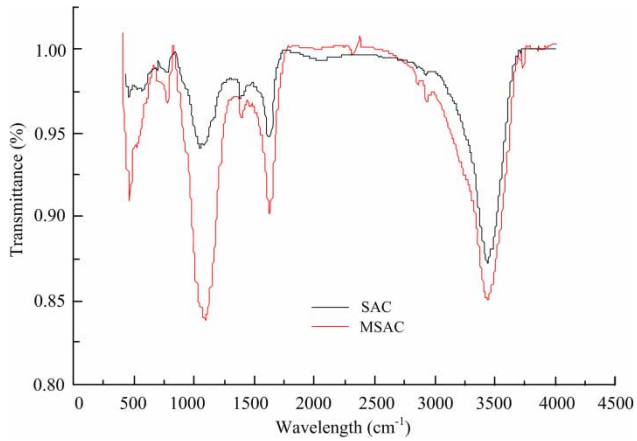

Figure 3 | FTIR curves of SAC and MSAC.

Downloaded from http://iwaponline.com/jwrd/article-pdf/11/1/97/842448/jwrd0110097.pdf
by guest

were found on the MSAC, which were more likely to provide a large number of active sites to interact with AMX. In addition, the peaks around 467 and 746 cm^{-1} were attributed to the stretching vibration of Ti-O-Ti and bending vibration of Ti-O-C, respectively (Natarajan *et al.* 2017), which were crucial in promoting photocatalytic degradation of AMX (Li *et al.* 2019a).

Removal performances

Effect of AC dosages

The effects of MSAC or SAC dosages (1–8 g/L) on AMX removal were studied at initial AMX concentration, pH, temperature, and contact time of 30 mg/L, 8.0, 25 °C and 180 min, respectively. As shown in Figure 4(a), when the MSAC dosage increased from 1.0 to 5.0 g/L, the removal rate of AMX gradually increased from 41.17 to 88.19%, and then remained relatively stable with the further increase of MSAC dosage. Similarly, AMX removal rate increased from 17.2 to 72.4% at SAC dosages of 1.0–6.0 g/L. In this study, as the dosages of SAC or MSAC increased, the improvement in AMX removal rate was mainly due to the increase in the number of available active sites (Chowdhury *et al.* 2019). Additionally, the higher removal rates of AMX by MSAC than SAC may be related to the synergistic effect of adsorption and photocatalysis.

Effect of initial concentrations

The effects of initial concentrations on AMX removal were conducted by varying AMX concentrations from 10 to 90 mg/L, and other parameters were controlled at pH 8.0, temperature 25 °C, and contact time 180 min. The result is presented in Figure 4(b). The removal rate went up from 73.7 to 88.19% when the initial AMX concentration increased from 10 to 30 mg/L. However, as the initial AMX concentration further increased to 90 mg/L, the removal rate first decreased and then stabilized at 70.8%. The increase in removal rate may be positively related to an enhancement of concentration gradient, which led to an increase in the driving force for adsorption (Chowdhury *et al.* 2019). In the current research, since the MSAC dosage remained constant during the adsorption process, the number of available active sites and photocatalysts was fixed. When the initial AMX concentration increased to a certain limit, the surface binding sites of MSAC reached saturation resulting in a reduction in AMX removal rate. In addition, SAC had a similar change trend to MSAC, and the removal rate of SAC to AMX at any initial AMX concentration was lower than that of MSAC. It could be speculated that the physical and chemical properties of MSAC were improved through combining modification.

Effect of pH

Figure 4(c) shows the effect of pH on AMX adsorption onto MSAC or SAC. It can be found that the initial pH had obvious influences on the removal performance of AMX. Taking MSAC as an example, the removal rates of AMX first increased and then decreased sharply, and the optimum removal rate (88.19%) appeared at pH 8.0. It is also seen from Figure 4(c) that the MSAC showed superior AMX removal rate than SAC at any pH value, indicating that the removal performance of MSAC to AMX was enhanced due to combining modification. The pH 8.0 was selected for the following kinetic, isotherm and thermodynamic experiments.

In this study, the surface charges distribution of AMX or AC samples and the surface property of nano-TiO_2 particles may be affected by strong acid or alkali conditions, which changed the electrostatic interaction and photocatalytic effect of MSAC on AMX. As is reported, the dissociation constants of carboxyl (pKa_1), amino (pKa_2) and hydroxyl (pKa_3) in AMX molecule were 2.68, 7.49 and 9.63, respectively (Goddard *et al.* 1996). In an acidic environment (pH 2.0–6.0), active groups such as carboxyl, amino and hydroxyl in AMX existed in the forms of -COOH/-COO^-, -NH_3^+ and -OH, respectively, which was of benefit for increasing the electrostatic affinity between AMX and AC samples (Pezoti *et al.* 2016). The reduction of AMX removal rate at pH 10.0 may be attributed to the electrostatic repulsion of AMX molecules by the AC samples, because both carboxyl and amine groups were deprotonated under basic conditions, making AMX negatively charged (Moussavi *et al.* 2013).

Effect of contact time

The effect of contact time on AMX removal was evaluated over a time range of 15–180 min. As shown in Figure 4(d),

Downloaded from http://iwaponline.com/jwrd/article-pdf/11/1/97/842448/jwrd0110097.pdf
by guest

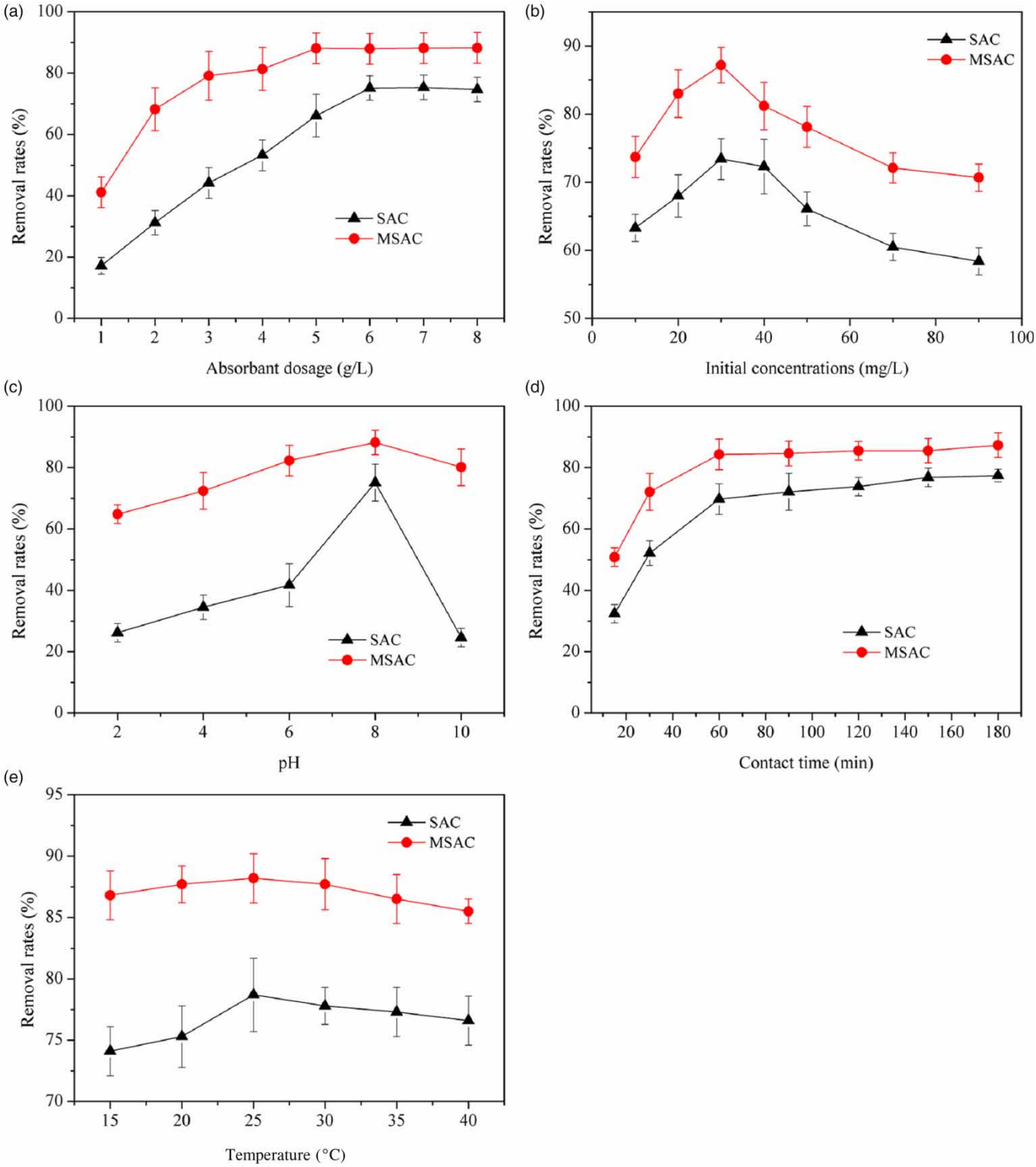

Figure 4 | Effect of: (a) AC dosages, (b) initial concentrations, (c) pH, (d) contact time, and (e) temperature on adsorption of AMX onto MSAC. Error bars represent the range of data from duplicate experiments.

Downloaded from http://iwaponline.com/jwrd/article-pdf/11/1/97/842448/jwrd0110097.pdf
by guest

the adsorption of AMX onto MSAC reached equilibrium at 60 min. In the first 60 min a sharp increase in AMX removal rate from 55.8 to 84.3% was observed, indicating that the adsorption process of AMX onto MSAC was very fast. However, further increase in contact time after equilibration did not change the removal rate of AMX. This is because there were many available binding sites on the surface of MSAC at the initial stage, nevertheless, with the increase of contact time, MSAC underwent a certain adsorption process, and the active sites were occupied by AMX molecules and reached saturation (Chitongo *et al.* 2019).

Effect of temperature

The effect of temperature on AMX removal was conducted at 15–40 °C, and the result is shown in Figure 4(e). The removal rate of AMX increased and reached the highest at 25 °C, and then declined with further increase in temperature. In this study, the maximum removal rate of AMX onto MSAC was 88.19%. This may be due to the fact that the kinetic energy of AMX molecules was low at lower temperatures, leading to the contact between the active sites on the MSAC and the AMX molecules being reduced. At higher temperatures, the kinetic energy of AMX molecules exceeded the attractiveness of MSAC to AMX, resulting in the decrease of removal rates (Chowdhury *et al.* 2019).

Adsorption kinetics studies

The kinetic models, including pseudo-first order (PFO), pseudo-second order (PSO) and intra-particle diffusion (IPD), were used for fitting the experimental data. The linear forms of PFO, PSO and IPD models are determined by Equations (4)–(6), respectively (Simonin 2016):

$$\ln(q_e - q_t) = \ln q_e - k_1 t \tag{4}$$

$$t/q_t = 1/k_2 q_e^2 + t/q_e \tag{5}$$

$$q_t = k_{ip} t^{1/2} + C \tag{6}$$

where k_1(1/min) and k_2 (g/(mg·min)) are the rate constant of PFO and PSO, respectively. The k_{ip} ((mg·min$^{1/2}$)/g) is diffusion rate constant in particles, and C is constant.

The fitting results and parameters obtained from the kinetic models are displayed in Figure 5 and Table 1, respectively. It can be seen from Table 1 that the correlation coefficients (R^2) of SAC and MSAC in the PSO model were 0.9967 and 0.9985, respectively, which were higher than that of the PFO and the IPD models. Meanwhile, the calculated q_e value (q_e^{cal}) by PSO model were closer to the experimental q_e value ($q_e^{\exp}$). Therefore, these results indicated that the PSO model was more reasonable for describing the adsorption process of AMX onto the SAC and MSAC. According to literature (Guo *et al.* 2014), the PSO model suggested that the adsorption of AMX onto the MSAC was mainly a chemisorption process. As shown in Table 1, the R^2 values of PFO and IPD models were >0.79, suggesting that the physisorption and intra-particle diffusion may contribute to the adsorption process (Chitongo *et al.* 2019). The same conclusion was also drawn from Figure 5. In this study, the straight line in Figure 5(c) did not pass through the origin of the coordinate, indicating that there was a certain degree of boundary layer adsorption.

Adsorption isotherm models

Adsorption isotherm is very important for the equilibrium and adsorption behavior of adsorbates onto AC samples (Simonin 2016). Therefore, the Langmuir, Freundlich and Temkin isotherm models were used for fitting the experimental results. A linear form of Langmuir equation is expressed as follows:

$$C_e/q_e = 1/k_L q_m + C_e/q_m \tag{7}$$

where k_L(L/mg) is the Langmuir constant related to the adsorption energy, and q_m (mg/g) is theoretical maximum AMX adsorption amount. The q_m and k_L values are deduced from the slope and intercept of the linear plot of C_e/q_e against C_e, respectively.

The nature of Langmuir isotherm can be further explained by separation factor (R_L) as given below:

$$R_L = 1/(1 + k_L C_0) \tag{8}$$

R_L is usually used to predict the adsorption efficiency. Adsorption is unfavorable when $R_L > 1$; favorable when $0 < R_L < 1$; while $R_L = 1$ indicates linearity.

Downloaded from http://iwaponline.com/jwrd/article-pdf/11/1/97/842448/jwrd0110097.pdf
by guest

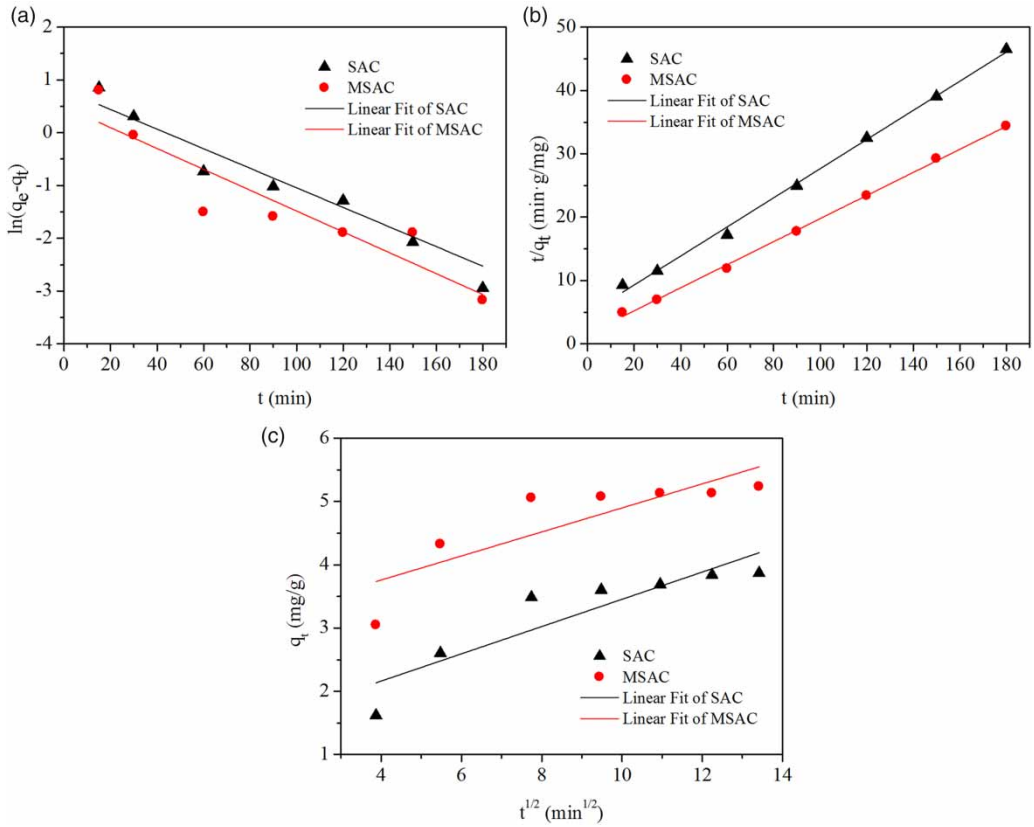

Figure 5 | Adsorption kinetics of AMX removal by SAC and MSAC: (a) PFO model, (b) PSO model and (c) IPD model.

Table 1 | Kinetics parameters for the adsorption of AMX onto SAC and MSAC

Kinetic models	Parameters	SAC	MSAC
Pseudo-first order	k_1	0.0185	0.0198
	k_e^{cal}	2.2477	1.6351
	R^2	0.9448	0.8298
Pseudo-second order	k_2	0.0113	0.0211
	q_e^{cal}	4.3516	5.4915
	R^2	0.9967	0.9985
Intra-particle diffusion	k_{ip}	0.2154	0.1900
	C	1.2998	0.3000
	R^2	0.791	0.6488

The Freundlich isotherm model is used to describe a multilayer adsorption process of adsorbates onto AC samples (Banerjee *et al.* 2016). A linear form of Freundlich equation is shown in Equation (9):

$$\ln q_e = \ln k_F + \ln C_e/n \tag{9}$$

where the k_F ((mg/g·(L/mg)$^{1/n}$) is Freundlich constant, and n is the adsorption intensity. The k_F and n are obtained from the slope and intercept of the graph of $\ln q_e$ versus $\ln C_e$. When $n = 1$, the adsorption process is linear; when $n < 1$, it is basically chemical; when $n > 1$, it is basically physical (Pezoti *et al.* 2016).

The Temkin isotherm model is mainly used to describe the electrostatic interaction and related heat between the adsorbates and the AC samples during the chemisorption process. The linear equation of Temkin isotherm is given below:

$$q_e = (RT/b_T)\ln k_T + (RT/b_T)\ln C_e \tag{10}$$

where k_T(L/mg) is the Temkin isotherm equilibrium binding constant, and b_T (J/mol) is the Temkin isotherm constant showing variation of adsorption energy; T(K) represents the absolute temperature, and R(J/(mol·K)) is the universal gas constant, 8.314. k_T and b_T are determined by the slope and intercept in the plot of q_e against $\ln C_e$, respectively.

Downloaded from http://iwaponline.com/jwrd/article-pdf/11/1/97/842448/jwrd0110097.pdf
by guest

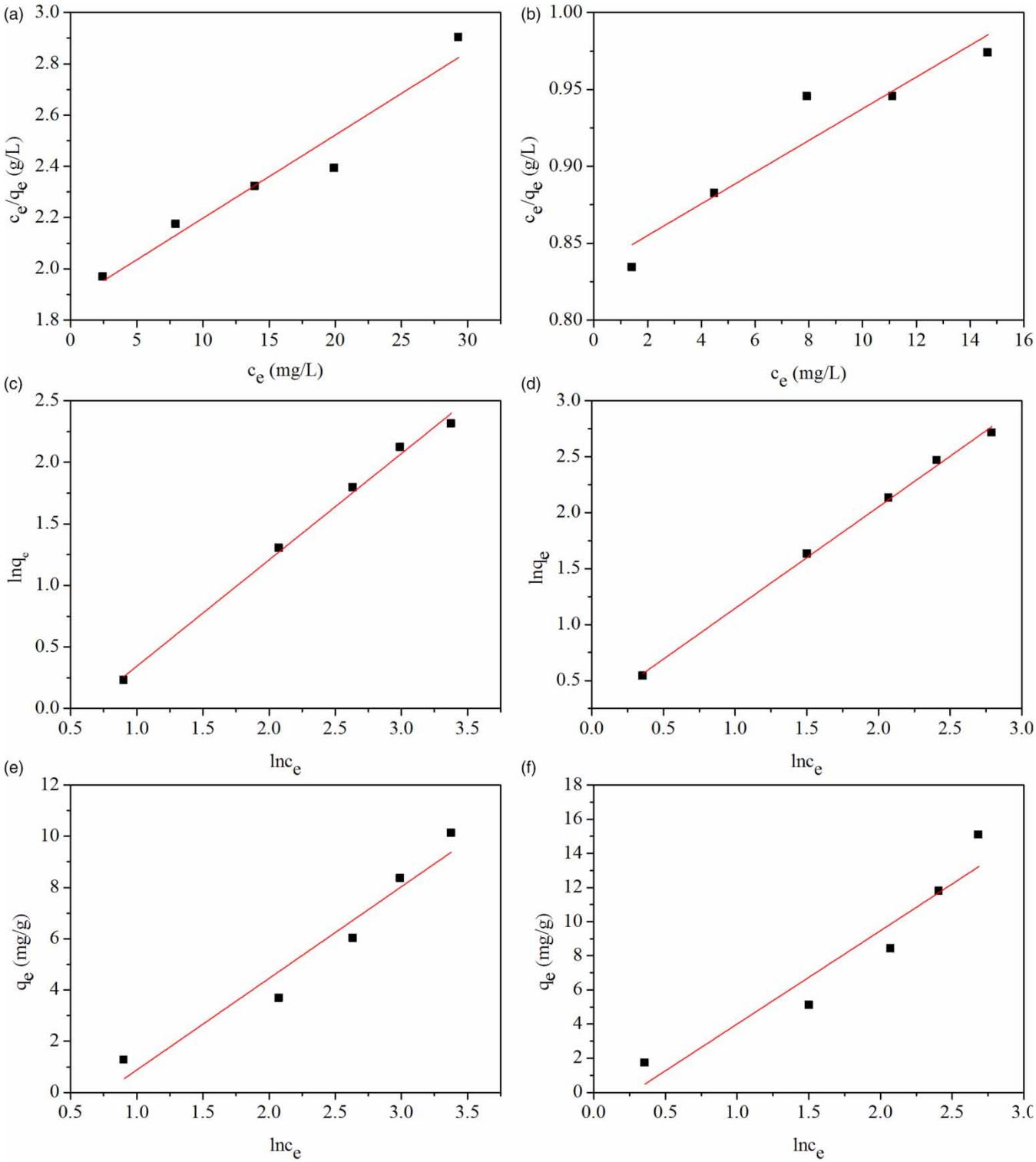

Figure 6 | (a) Langmuir isotherm, (c) Freundlich isotherm, (e) Temkin isotherm models of AMX onto SAC, and (b) Langmuir isotherm, (d) Freundlich isotherm, (f) Temkin isotherm models of AMX onto MSAC.

Downloaded from http://iwaponline.com/jwrd/article-pdf/11/1/97/842448/jwrd0110097.pdf
by guest

The fitted results of the experimental data and the linear models and the corresponding parameters are shown in Figure 6 and Table 2, respectively. Based on the R^2 (>0.85) described in Table 2, it is demonstrated that these three models all fitted well with the adsorption processes of AMX onto the MSAC and SAC. It can also be seen that the Freundlich model showed a higher fitting degree than the Langmuir and Temkin models, because the R^2 value of Freundlich isotherm was closer to 1. Simultaneously, the n value for AMX adsorption onto the MSAC or SAC was > 1, which suggested the adsorption process was multilayered and probably occurred on heterogenous surfaces (Chowdhury *et al.* 2019). Moreover, the q_m and R_L of the MSAC, as predicted by Langmuir isotherm, were higher than that of the SAC. In this study, the qm and R_L values of MSAC were 97.087 mg/g and 0.73, respectively, indicating that the adsorption of AMX onto the MSAC was favorable. The results of k_T and b_T implied that as the surface coverage of MSAC enhanced, the heat of adsorption decreased.

Adsorption thermodynamics

Thermodynamics studies were evaluated by thermodynamic parameters, including entropy change ΔS (kJ/mol K), enthalpy change ΔH (kJ/mol), and Gibb's free energy change ΔG (kJ/mol). The ΔG is determined by Equations (11) and (12) (Mondal *et al.* 2016):

$$\Delta G = -\mathrm{RT} \times \ln (C_a/C_e) \tag{11}$$

$$\Delta G = \Delta H - T\Delta S \tag{12}$$

Table 2 | Adsorption isotherm parameter of AMX removal by SAC and MSAC

Isotherm models	Parameters	SAC	MSAC
	k_L (L/mg)	0.017	0.012
Langmuir model	q_m (mg/g)	30.845	97.087
	R_L	0.658	0.73
	R^2	0.9324	0.8738
Freundlich model	k_F (L/mg)	0.594	1.27
	n	1.157	1.103
	R^2	0.9935	0.9971
Temkin model	k_T (L/g)	0.47	0.765
	b_T (J/mol)	692.543	453.096
	R^2	0.9259	0.8828

Table 3 | Thermodynamic parameters at different temperatures

Samples	T(K)	ΔG(kJ/mol)	ΔH (kJ/mol)	ΔS (kJ/(mol·K)
SAC	288.15	1.351	5.334	13.820
	293.15	1.283		
	298.15	1.214		
MSAC	288.15	–0.698	7.497	28.438
	293.15	–0.840		
	298.15	–0.982		

where C_a (mg/L) is the AMX concentration on MSAC or SAC in equilibrium. The ΔS and ΔH can be calculated from the slope and intercept of the linear plot of ΔG versus T, respectively.

As shown in Table 3, the ΔG for the sorption of AMX onto SAC was positive, while the ΔG of MSAC was negative at three adsorption temperatures. The $\Delta G < 0$ meant that the adsorption process of AMX on the surface of MSAC was spontaneous (Bedia *et al.* 2017). Simultaneously, an increase in the absolute value of ΔG showed that the spontaneity was enhanced at high temperature. The positive value of ΔH indicated that the diffusion and adsorption of AMX on MSAC or SAC was an endothermic process (Luo *et al.* 2017). Furthermore, the positive value of ΔS also confirmed an increase of randomness at the interface of MSAC and AMX (Chowdhury *et al.* 2019). In this study, the enhancement of functional groups and the development of pore structures on the surface of MSAC may be the main reasons for the different adsorption parameters of MSAC and SAC.

CONCLUSIONS

The MSAC was obtained by combining modification of walnut shell and nano-TiO_2, and it was applied to adsorb AMX from aqueous solution. The highest AMX removal rate of 88.19% was observed at an MSAC dosage of 5.0 g/L, an initial AMX concentration of 30 mg/L, a temperature of 25 °C, a contact time of 180 min, and a pH of 8.0. The MSAC had better physicochemical properties than SAC in terms of pore structure (especially micropores), and surface functional groups (C-O, C = O, Ti-O-Ti), so it was more favorable for the removal of AMX. The adsorption of AMX onto MSAC fitted well with the PSO kinetic model

Downloaded from http://iwaponline.com/jwrd/article-pdf/11/1/97/842448/jwrd0110097.pdf
by guest

and Freundlich isotherm model. The maximum monolayer adsorption capacity of MSAC (97.087 mg/g) was much higher than that of SAC (30.845 mg/g). In addition, the adsorption thermodynamics study showed the adsorption process was endothermic, feasible and spontaneous.

ACKNOWLEDGEMENTS

This work was financially supported by the Nanjing Forestry University Youth Innovation Fund (CX2017025), National Natural Science Foundation of China (51608272), and Undergraduate Practical Innovation Training Program Project (2019NFUSPITP0487).

DATA AVAILABILITY STATEMENT

All relevant data are included in the paper or its Supplementary Information.

REFERENCES

Anisuzzaman, S. M., Joseph, C. G., Krishnaiah, D., Bono, A., Suali, E., Abang, S. & Fai, L. M. 2016 Removal of chlorinated phenol from aqueous media by guava seed (Psidium guajava) tailored activated carbon. *Water Resour. Ind.* **16**, 29–36.

APHA 2001 *Standard Methods for the Examination of Water and Wastewater*, 20th edn. American Public Health Association, Washington, DC, USA.

Baere, S. D. & Backer, P. D. 2007 Quantitative determination of amoxicillin in animal feed using liquid chromatography with tandem mass spectrometric detection. *Anal. Chim. Acta* **586**, 319–325.

Banerjee, S., Mukherjee, S., LaminKa-ot, A., Joshi, S. R., Mandal, T. & Halder, G. 2016 Biosorptive uptake of Fe^{2+}, Cu^{2+} and As^{5+} by activated biochar derived from Colocasia esculenta: isotherm, kinetics, thermodynamics, and cost estimation. *J. Adv. Res.* **7**, 597–610.

Bedia, J., Belver, C., Ponce, S., Rodriguez, J. & Rodriguez, J. J. 2017 Adsorption of antipyrine by activated carbons from $fecl_3$-activation of Tara Gum. *Chem. Eng. J.* **333**, 58–65.

Calisto, V., Ferreira, C. I. A., Oliveira, J. A. B. P., Otero, M. & Esteves, V. I. 2015 Adsorptive removal of pharmaceuticals from water by commercial and waste-based carbons. *J. Environ. Manage.* **152**, 83–90.

Chitongo, R., Opeolu, B. O. & Olatunji, O. S. 2019 Abatement of amoxicillin, ampicillin, and chloramphenicol from aqueous solutions using activated carbon prepared from grape slurry. *Clean-Soil Air Water* **47**, 1800077. http://doi.org/10.1002/clen.201800077.

Chowdhury, S., Sikder, J., Mandal, T. & Halder, G. 2019 Comprehensive analysis on sorptive uptake of enrofloxacin by activated carbon derived from industrial paper sludge. *Sci. Total Environ.* **665**, 438–452.

Devi, P. & Saroha, A. K. 2017 Utilization of sludge based adsorbents for the removal of various pollutants: a review. *Sci. Total Environ.* **578**, 16–33.

Fazal, T., Razzaq, A., Javed, F., Hafeez, A., Rashid, N., Amjad, U. S., Ur Rehman, M. S., Faisal, A. & Rehman, F. 2019 Integrating adsorption and photocatalysis: a cost effective strategy for textile wastewater treatment using hybrid biochar-TiO_2 composite. *J. Hazard. Mater.* **390**, 121623.

Goddard, A. F., Jessa, M. J., Barrett, D. A., Shaw, P. N., Idstrom, J. P., Cederberg, C. & Spiller, R. C. 1996 Effect of omeprazole on the distribution of metronidazole, amoxicillin, and clarithromycin in human gastric juice. *Gastroenterology* **111**, 358–367.

Gokce, Y. & Aktas, Z. 2014 Nitric acid modification of activated carbon produced from waste tea and adsorption of methylene blue and phenol. *Appl. Surf. Sci.* **313**, 352–359.

Gonzalez-Pleiter, M., Gonzalo, S., Rodea-Palomares, I., Leganes, F., Rosal, R., Boltes, K., Marco, E. & Fernandez-Pinas, F. 2013 Toxicity of five antibiotics and their mixtures towards photosynthetic aquatic organisms: implications for environmental risk assessment. *Water Res.* **47**, 2050–2064.

Guo, X., Du, B., Wei, Q., Yang, J., Hu, L., Yan, L. & Xu, W. 2014 Synthesis of amino functionalized magnetic graphenes composite material and its application to remove Cr(VI), Pb(II), Hg(II), Cd(II) and Ni(II) from contaminated water. *J. Hazard. Mater.* **278**, 211–220.

Hassan, M., Naidu, R., Du, J. H., Liu, Y. J. & Qi, F. J. 2020 Critical review of magnetic biosorbents: their preparation, application, and regeneration for wastewater treatment. *Sci. Total Environ.* **702**, 134893. http://doi.org/10.1016/j.scitotenv.2019.134893.

Jaria, G., Calisto, V., Silva, C. P., Gil, M. V., Otero, M. & Esteves, V. I. 2019a Obtaining granular activated carbon from paper mill sludge – A challenge for application in the removal of pharmaceuticals from wastewater. *Sci. Total Environ.* **653**, 393–400.

Jaria, G., Silva, C. P., Oliveira, J. A. B. P., Santos, S. M., Gil, M. V., Otero, M., Calisto, V. & Esteves, V. I. 2019b Production of highly efficient activated carbons from industrial wastes for the removal of pharmaceuticals from water – A full factorial design. *J. Hazard. Mater.* **370**, 212–218.

Jin, S. C., Park, S. H., Jung, S. C., Ryu, C. & Park, Y. K. 2016 Production and utilization of biochar: a review. *J. Ind. Eng. Chem.* **40**, 1–15.

Kumari, M. & Kumar, A. 2020 Human health risk assessment of antibiotics in binary mixtures for finished drinking water. *Chemosphere.* **240**, 124864.

Downloaded from http://iwaponline.com/jwrd/article-pdf/11/1/97/842448/jwrd0110097.pdf
by guest

Li, Y. L., Li, Y. L., Li, L. P., Shi, X. J. & Wang, Z. 2016 Preparation and analysis of activated carbon from sewage sludge and corn stalk. *Adv. Powder Technol.* **27**, 684–691.

Li, H., Hu, J., Wang, X. & An, L. 2019a Development of a bio-inspired photo-recyclable feather carbon adsorbent towards removal of amoxicillin residue in aqueous solutions. *Chem. Eng. J.* **373**, 1380–1388.

Li, L., Zhong, D., Xu, Y. & Zhong, N. 2019b A novel superparamagnetic micro-nano-bio-adsorbent PDA/Fe_3O_4/BC for removal of hexavalent chromium ions from simulated and electroplating wastewater. *Environ. Sci. Pollut. R.* **26**, 23981–23993.

Li, Q., Jia, R., Shao, J. & He, Y. 2019c Photocatalytic degradation of amoxicillin via TiO_2 nanoparticle coupling with a novel submerged porous ceramic membrane reactor. *J. Clean. Prod.* **209**, 755–761.

Liu, T., Li, Y., Peng, N., Lang, Q., Xia, Y., Gai, C., Zheng, Q. & Liu, Z. 2017a Heteroatoms doped porous carbon derived from hydrothermally treated sewage sludge: structural characterization and environmental application. *J. Environ. Manage.* **197**, 151–158.

Liu, Y., Kang, X., Li, X., Wang, Z. & Jing, Z. 2017b Performance and mechanism of sludge dewaterability enhanced by potassium ferrate pretreatment and calcium chloride addition. *J. Water Reuse Desal.* **7**, 136–141.

Luo, H., Zhang, S., Li, X., Liu, X., Xu, Q., Liu, J. & Wang, Z. 2017 Tannic acid modified Fe_3O_4 core-shell nanoparticles for adsorption of Pb^{2+} and Hg^{2+}. *J. Taiwan Inst. Chem. E.* **72**, 163–170.

Mondal, S., Bobde, K., Aikat, K. & Halder, G. 2016 Biosorptive uptake of ibuprofen by steam activated biochar derived from mung bean husk: equilibrium, kinetics, thermodynamics, modeling and eco-toxicological studies. *J. Environ. Manage.* **182**, 581–594.

Moussavi, G., Alahabadi, A., Yaghmaeian, K. & Eskandari, M. 2013 Preparation, characterization and adsorption potential of the NH_4Cl-induced activated carbon for the removal of amoxicillin antibiotic from water. *Chem. Eng. J.* **217**, 119–128.

Natarajan, T. S., Lee, J. Y., Bajaj, H. C., Jo, W. K. & Tayade, R. J. 2017 Synthesis of multiwall carbon nanotubes/TiO_2 nanotube composites with enhanced photocatalytic decomposition efficiency. *Catal. Today* **282**, 13–23.

Pal, A., Thu, K., Mitra, S., El-Sharkawy, I. I., Saha, B. B., Kil, H. S., Yoon, S. H. & Miyawaki, J. 2017 Study on biomass derived activated carbons for adsorptive heat pump application. *Int. J. Heat Mass Transf.* **110**, 7–19.

Pezoti, O., Cazetta, A. L., Bedin, K. C., Souza, L. S., Martins, A. C., Silva, T. L., Santos Junior, O. O., Visentainer, J. V. & Almeida, V. C. 2016 NaOH-activated carbon of high surface area produced from guava seeds as a high-efficiency adsorbent for amoxicillin removal: kinetic, isotherm and thermodynamic studies. *Chem. Eng. J.* **288**, 778–788.

Salame, I. I. & Bandosz, T. J. 2003 Role of surface chemistry in adsorption of phenol on activated carbons. *J. Colloid Interf. Sci.* **264**, 307–312.

Silva, C. P., Jaria, G., Otero, M., Esteves, V. I. & Calisto, V. 2018 Waste-based alternative adsorbents for the remediation of pharmaceutical contaminated waters: has a step forward already been taken? *Bioresour. Technol.* **250**, 888–901.

Silva, C. P., Jaria, G., Otero, M., Esteves, V. I. & Calisto, V. 2019 Adsorption of pharmaceuticals from biologically treated municipal wastewater using paper mill sludge-based activated carbon. *Environ. Sci. Pollut. R.* **26**, 13173–13184.

Silvestri, S., Stefanello, N., Sulkovski, A. A. & Foletto, E. L. 2019 Preparation of TiO_2 supported on MDF biochar for simultaneous removal of methylene blue by adsorption and photocatalysis. *J. Chem. Technol. Biot.* **95**, 2723–2729. http:// dio.org/10.1002/jctb.6279.

Simonin, J. P. 2016 On the comparison of pseudo-first order and pseudo-second order rate laws in the modeling of adsorption kinetics. *Chem. Eng. J.* **300**, 254–263.

Sullivan, G. L., Prigmore, R. M., Knight, P. & Godfrey, A. R. 2019 Activated carbon biochar from municipal waste as a sorptive agent for the removal of polyaromatic hydrocarbons (PAHs), phenols and petroleum based compounds in contaminated liquids. *J. Environ. Manage.* **251**, 109551. http:// dio.org/10.1016/j.jenvman.2019.109551.

Wang, Z., Zhong, M. & Chen, L. 2016 Coal-based granular activated carbon loaded with MnO_2 as an efficient adsorbent for removing formaldehyde from aqueous solution. *Desalin. Water Treat.* **57**, 13225–13235.

Wang, L., Chang, Y. & Liu, Q. 2019 Fate and distribution of nutrients and heavy metals during hydrothermal carbonization of sewage sludge with implication to land application. *J. Clean. Prod.* **225**, 972–983.

Yang, X., Xu, G., Yu, H. & Zhang, Z. 2016 Preparation of ferric-activated sludge-based adsorbent from biological sludge for tetracycline removal. *Bioresour. Technol.* **211**, 566–573.

Yao, H., Lu, J., Wu, J., Lu, Z., Wilson, P. C. & Shen, Y. 2013 Adsorption of fluoroquinolone antibiotics by wastewater sludge biochar: role of the sludge source. *Water Air Soil Poll.* **224**, 1370–1379.

Yu, Z., Gao, Q., Zhang, Y., Wang, D., Nyalala, I. & Chen, K. 2019 Production of activated carbon from sludge and herb residue of traditional Chinese medicine industry and its application for methylene blue removal. *Bioresources* **14**, 1333–1346.

Zhang, D., Huo, P. & Liu, W. 2016 Behavior of phenol adsorption on thermal modified activated carbon. *Chinese J. Chem. Eng.* **24**, 446–452.

First received 8 July 2020; accepted in revised form 27 September 2020. Available online 19 November 2020

Downloaded from http://iwaponline.com/jwrd/article-pdf/11/1/97/842448/jwrd0110097.pdf
by guest